Supplementary Lecture Notes for Accelerator Physics

SUNYSB: PHY684.02
Fall, 2004
SUNYSB, Stony Brook, NY

William W. MacKay
Brookhaven National Laboratory

"Faiëmo i lûmetti in sciä ciappa do leugo" Press

Table of Contents

1

Canonical Momentum for the Lorentz Force

For a conservative force, the work done by the force in moving from point P_1 to point P_2 is independent of the path taken:

$$\int_{P_1}^{P_2} \vec{F} \cdot d\vec{r} \quad \text{is invariant,}$$

or more succinctly

$$\oint \vec{F} \cdot d\vec{r} = 0 \tag{1.1}$$

from which by use of Stoke's theorem we get in differential form

$$\nabla \times \vec{F} = 0. \tag{1.2}$$

From basic mechanics we learned that forces which only depend on position and not the velocity of the particle being worked upon are conservative. Examples of such forces are those from gravitational and static electric fields. When there are magnetic fields present the Lorentz force can depend on velocity:

$$\frac{d\vec{p}}{dt} = \vec{F} = q(\vec{E} + \vec{v} \times \vec{B}), \tag{1.3}$$

and is not always conservative. Taking the curl of the Lorentz force yields:

$$\begin{aligned}
\nabla \times \vec{F} = \nabla \times \frac{d\vec{p}}{dt} &= q(\nabla \times \vec{E} + \nabla \times (\vec{v} \times \vec{B})) \\
&= -q\frac{\partial \vec{B}}{\partial t} + q\left[(\vec{B} \cdot \nabla)\vec{v} - (\vec{v} \cdot \nabla)\vec{B} + (\nabla \cdot \vec{B})\vec{v} - (\nabla \cdot \vec{v})\vec{B}\right] \\
&= -q\frac{\partial \vec{B}}{\partial t} - q\left[(\vec{v} \cdot \nabla)\vec{B}\right] \\
&= -q\left[\frac{\partial \vec{B}}{\partial t} + \frac{\partial \vec{B}}{\partial x}\frac{dx}{dt} + \frac{\partial \vec{B}}{\partial y}\frac{dy}{dt} + \frac{\partial \vec{B}}{\partial z}\frac{dz}{dt}\right] \\
&= -q\frac{d\vec{B}}{dt} \\
&= -\frac{d}{dt}(\nabla \times q\vec{A}).
\end{aligned} \tag{1.4}$$

Moving terms to the left side produces

$$\nabla \times \frac{d\vec{p}}{dt} + \frac{d}{dt}(\nabla \times q\vec{A}) = 0, \tag{1.5}$$

which after reordering the differentiation becomes

$$\nabla \times \left[\frac{d}{dt}\left(\vec{p} + q\vec{A}\right)\right] = 0. \tag{1.6}$$

If we define a new *canonical momentum* by

$$\vec{P} = \vec{p} + q\vec{A}, \tag{1.7}$$

then the corresponding *canonical force*

$$\vec{F}_{\text{can}} = \frac{d\vec{P}}{dt} \tag{1.8}$$

is conservative.

2

Alternative Derivation of Eq. (CM: 3.75)

In going from Eq. (3.60) to Eq. 3.75 of Conte and MacKay[1], I have not been quite rigorous enough in applying the canonical transformation; hence it was necessary to use a bit of hand waving to add an extra term of $+1$ to the dz/ds equation in Eq. (3.75). When we are more careful with the canonical transformation, we find that the Hamiltonian in Eqs. (3.64 and 3.72) must have an additional term of $+\delta$.

Eq. (3.60) may be rewritten using the paraxial approximation as

$$H_1(x,x',y,y',t,-U/p_0;s) = -\frac{q}{p_0}A_s - \left(1+\frac{x}{\rho}\right)\sqrt{\left(\frac{U}{p_0 c}\right)^2 - \left(\frac{mc}{p_0}\right)^2 - x'^2 - y'^2}.$$

We would like to transform to a Hamiltonian

$$\mathcal{H}(x,x',y,y',z,\delta;s) = H_1(x,x',y,y',t,-U/p_0;s) + \frac{\partial F_2(t,\delta;s)}{\partial s},$$

where F_2 is a generating function for the canonical transformation (See Appendix C.) with

$$z = \frac{\partial F_2}{\partial \delta}, \quad \text{and} \quad -\frac{U}{p_0} = \frac{\partial F_2}{\partial t}.$$

Since

$$\delta = \frac{\Delta p}{p_0} = \frac{U_0^2}{p_0^2 c^2}\frac{\Delta U}{U_0} = \frac{1}{\beta_0^2}\frac{\Delta U}{U_0},$$

the relation between $\frac{U}{p_0}$ and δ is

$$\frac{U}{p_0} = \frac{c}{\beta}(1+\beta^2\delta).$$

A good candidate for the generating function is

$$\begin{aligned} F_2(t,\delta;s) &= \frac{U}{p_0}(t_0 - t) - \frac{s}{\beta_0^2} \\ &= \frac{c}{\beta_0}(1+\beta_0^2\delta)(t_0 - t) - \frac{s}{\beta_0^2} \\ &= \frac{c}{\beta_0}(1+\beta_0^2\delta)\left(\frac{s}{v_0} - t\right) - \frac{s}{\beta_0^2}, \end{aligned}$$

since $s = v_0 t_0$. Evaluating for z then gives

$$z = s - v_0 t,$$

as shown in Eq.(3.63). The additional term missing from Eq. (3.72) is then

$$\frac{\partial F_2}{\partial s} = \delta.$$

Thus we see that a more careful treatment leads to the desired answer without the extra hand waving.

References for Chapter 2

[1] M. Conte and W. W. MacKay, *An Introduction to the Physics of Particle Accelerators*, World Scientific, Singapore (1991).

3

Transverse Position Measurement

The most common method for measuring the transverse position of the a bunched beam is to sense the electric field with capacitive pickups. As the bunch travels down the beam pipe, image charges move along the inner surface of the pipe. (Here I am of course assuming that the beam pipe is made of metal.) From Gauss' law it is easy to see that the total charge moving along the pipe must be equal but of opposite sign to the charge in the bunch.

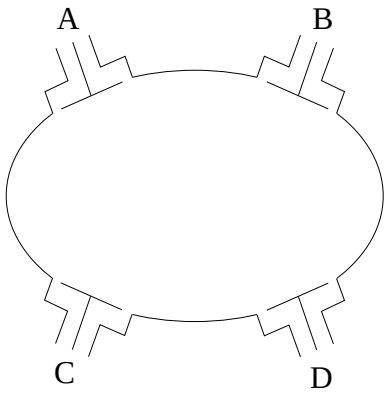

Figure. 3.1 Concept of a dual plane beam-button position monitor. The signals from each button are brought out to the readout electronics via high quality coaxial cables. Here the buttons have been placed as in a synchrotron light source to keep them out of the band of synchrotron radiation in the midplane.

One type monitor employs button shaped electrodes to sense the electric field strength at the surface of the chamber as shown in Fig. (3.1). Buttons are particularly used when the bunches are short as in electron accelerators. The short length of the electrode can limit the amount of induced charge if the bunches are longer than the radius of the button.

When the bunches are longer as in hadron accelerators, longer stripline electrodes are frequently used. Fig. (3.2) shows a shorted stripline monitor with a measured signal from the lower stripline.

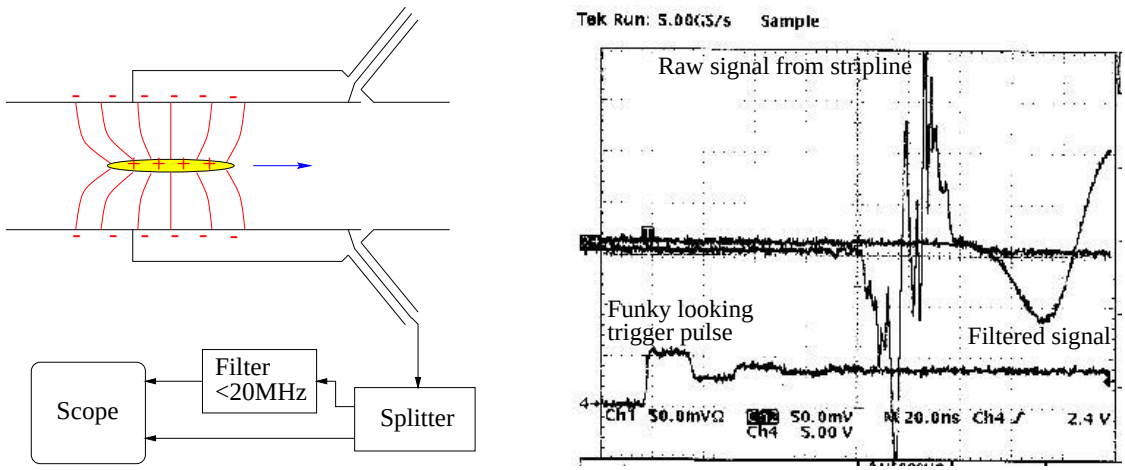

Figure. 3.2 Concept of a stripline beam position monitor. Induced currents on the wall are picked up on coaxial cables by using a small gap at the end of the stripline. The capacitive nature of such a pickup differentiates the bunch current. On the right are measurements of a fully stripped gold bunch passing through a stripline position monitor after being extracted from the AGS. As can be seen, there was quite a bit of structure in the bunch. (This was taken early in the commissioning of the extraction system.)

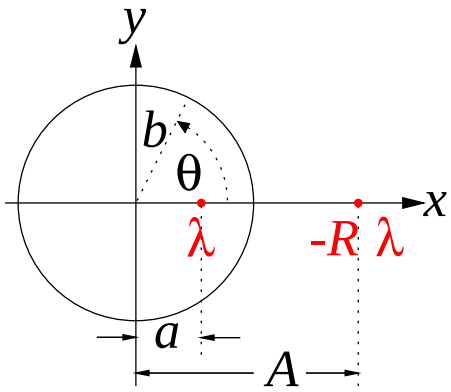

Figure. 3.3 Equipotential surface with line of charge density λ at radius a and an image line of charge of density $-R\lambda$ at radius A.

An estimate of the charge density on the inner surface of a cylindrical beam pipe of radius b can be made by treating the bunch as a line of charge of density λ at a distance a from the center of the pipe. Ignoring the pipe, a second line of image charge (line density: $-R\lambda$) can be placed parallel to the beam but at a distance A from the origin. We solve for distance A and the ratio R to have an equipotential surface on a cylinder of radius b. The equation for the potential lines of charge is then

$$V = \frac{\lambda}{2\pi\epsilon_0}\left[\ln\left(\sqrt{(x-a)^2+y^2}\right) - R\ln\left(\sqrt{(x-A)^2+y^2}\right)\right] + V_0. \qquad (3.1)$$

Rearranging terms produces

$$\frac{2\pi\epsilon_0}{\lambda}(V - V_0) = \frac{1}{2}\ln\frac{(x-a)^2 + y^2}{[(x-A)^2 + y^2]^R}. \tag{3.2}$$

After exponentiating, we may define

$$\alpha = e^{\frac{4\pi\epsilon_0}{\lambda}(V - V_0)} = \frac{(x-a)^2 + y^2}{[(x-A)^2 + y^2]^R}. \tag{3.3}$$

In order to have a cylindrical equipotential surface, we must have a quadratic equation, so $R = 1$, and

$$(x-a)^2 + y^2 = \alpha[(x-A)^2 + y^2].$$

Since the potential at $(x, y) = (b, 0)$ must be the same as at $(x, y) = (0, b)$, we can write

$$\alpha = \frac{(b-a)^2}{(A-b)^2} = \frac{a^2 + b^2}{A^2 + b^2}. \tag{3.4}$$

Solving for A gives the nontrivial answer

$$A = \frac{b^2}{a}.$$

(The other root is $A = a$ which just cancels the charge at $x = a$.) Transforming to polar coordinates ($x = r\cos\theta$, $y = r\sin\theta$) and evaluating the radial component of electric field at $r = b$ gives

$$E_r(r = b, \theta) = -\frac{\lambda}{2\pi\epsilon_0}\left[\frac{b^2 - a^2}{b(b^2 + a^2 - 2ab\cos\theta)}\right]. \tag{3.5}$$

Since the field is zero inside the conductor, the surface on the inner wall of the beam pipe must be

$$\sigma(\theta) = \epsilon_0 E_\perp = -\frac{\lambda}{2\pi}\left[\frac{b^2 - a^2}{b(b^2 + a^2 - 2ab\cos\theta)}\right]. \tag{3.6}$$

Now the charge per length on a stripline subtending the arc from θ_1 to θ_2 (See Fig. (3.4).) obtained by integrating

$$\begin{aligned}\frac{dq}{dz} &= -\frac{\lambda}{2\pi}\int_{\theta_1}^{\theta_2}\left[\frac{b^2 - a^2}{b(b^2 + a^2 - 2ab\cos\theta)}\right]d\theta \\ &= \frac{\lambda}{\pi}\tan^{-1}\left[\left(\frac{b+a}{b-a}\right)\tan\frac{\theta}{2}\right]\Bigg|_{\theta_1}^{\theta_2}.\end{aligned} \tag{3.7}$$

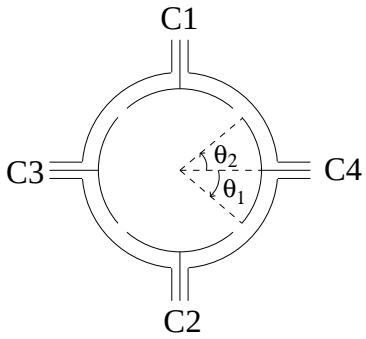

Figure. 3.4 Definition of angles of integration for stripline "C4".

For the opposite plate we can reverse the sign of a. The voltage induced across the coaxial cables will be proportional to the dq/dz on the stripline. To go further requires either a lot more algebra or invocation of a symbolic calculator such as MAPLE[3]. To first order in x/b we get

$$\frac{V_1 - V_2}{V_1 + V_2} = 4\frac{\sin\frac{\alpha}{2}}{\alpha}\frac{x}{b} + O\left(\frac{x^3}{b^3}\right) + O\left(\frac{xy^2}{b^3}\right). \tag{3.8}$$

where $\alpha = \theta_2 - \theta_1$, and we have replaced a by x. A somewhat more linear formula comes from

$$\ln\frac{V_1}{V_2} = 8\frac{\sin\frac{\alpha}{2}}{\alpha}\frac{x}{b} + O\left(\frac{x^3}{b^3}\right) + O\left(\frac{xy^2}{b^3}\right). \tag{3.9}$$

As an example, assume that the striplines subtend an angle of $\alpha = 70°$ ($\theta_1 = -35°$, $\theta_2 = 35°$) and a radius for the striplines of $b = 56.5$ mm, then we get to first order from Eq. (3.8): Fig. (3.5) shows typical signals from the four plates of a dual plane stripline with above dimensions.

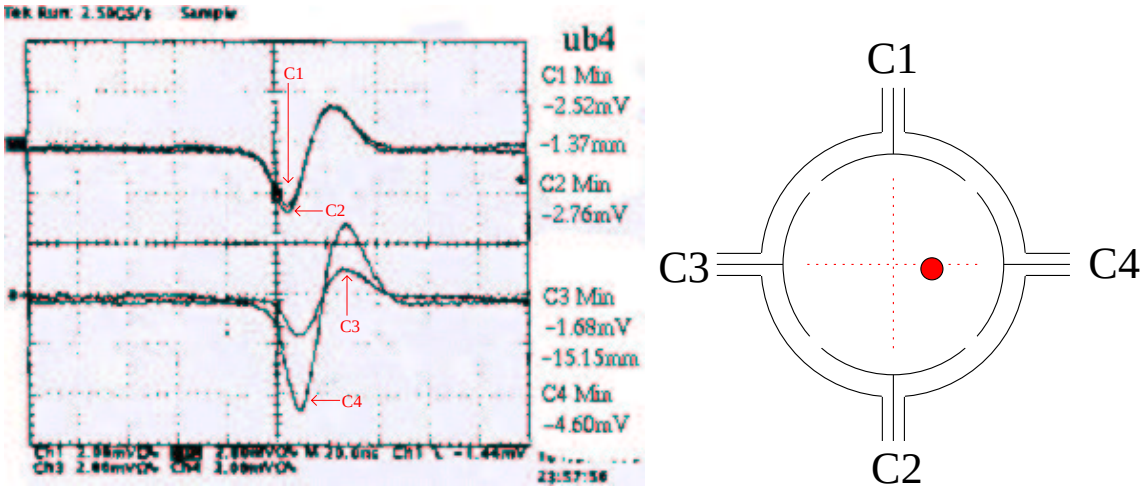

Figure. 3.5 Filtered signals from all four striplines of a two plane position monitor. The relative sizes of the voltages show that the beam was slightly down and to the right as indicated in the picture on the right. The positions were calculated using Eq. (3.9).

The accuracy of relative position measurements in a circular accelerator with a stripline monitor can be better than 10 μm when the signals are averaged over several turns.

References for Chapter 3

[1] R. E. Shafer, "Beam Position Monitoring", AIP Conf. Proc. 212, p. 26, New York (1990).

[2] R. E. Shafer, "Characteristics of Directional Coupler Beam Position Monitors", *IEEE Trans. on Nucl. Sci.*, Vol. NS-32, #5 p. 1933 (1985).

[3] B. W. Char et al., *Maple V First Leaves: A Tutorial Introduction* Springer-Verlag, New York (1992)

4

Schottky Signals

4.1 Coherent frequency spectra of bunched beams

4.1.1 A single Gaussian bunch

A Gaussian bunch of total charge q passing a pickup at location s will have a longitudinal profile

$$dQ(s,t) = \frac{q}{\sqrt{2\pi}\sigma_s}\, e^{\frac{-(s-vt)^2}{2\sigma_s}}\, ds, \tag{4.1}$$

where σ_s is the rms width of the distribution. The distribution of current passing the pickup is then

$$\begin{aligned} i(t) &= \frac{dQ}{dt} = v\,\frac{dQ}{ds} \\ &= \frac{qv}{\sqrt{2\pi}\sigma_s}\, e^{\frac{-(s-vt)^2}{2\sigma_s}} \\ &= \frac{q}{\sqrt{2\pi}\sigma_t}\, e^{\frac{-(t-t_0)^2}{2\sigma_t}}, \end{aligned} \tag{4.2}$$

where $t_0 = s/v$. For the following discussion, we will place the pickup at $s = 0$, so $t_0 = 0$. The harmonic content of the signal may be found from the Fourier transform[†] of the current:

$$\begin{aligned} \hat{\imath}(\omega) &= \frac{q}{\sqrt{2\pi}\sigma_t}\int_{-\infty}^{\infty} e^{-j\omega t}\, e^{-\frac{t^2}{2\sigma_t^2}}\, dt, \\ &= \frac{q}{\sqrt{2\pi}\sigma_t} e^{-\frac{\sigma_t^2\omega^2}{2}} \int_{-\infty}^{\infty} e^{-\frac{(t+j\sigma_t^2\omega)^2}{2\sigma_t^2}}\, dt, \\ &= q\, e^{-\frac{\sigma_t^2\omega^2}{2}}. \end{aligned} \tag{4.3}$$

So we find that the Fourier transform of a Gaussian distribution is again Gaussian with an rms width of $\sigma_\omega = 1/\sigma_t$. In the limit of an infinitesimally short bunch the

[†] Here I have used the engineering convention of $j = \sqrt{-1}$ to minimize confusion with the current i.

Gaussian distribution becomes

$$i(t) = \lim_{\sigma_t \to 0} \frac{q}{\sqrt{2\pi}\sigma_t} e^{-\frac{t^2}{2\sigma_t}} = q\,\delta(t), \tag{4.4}$$

and the spectral content becomes flat

$$\hat{\imath}(\omega) = q \int_{-\infty}^{\infty} e^{-j\omega t}\,\delta(t)\,dt = q. \tag{4.5}$$

4.1.2 Circulating bunches

The bunched beam current in a circular accelerator of circumference L with N_p equally spaced bunches may be approximated by

$$i(t) = \sum_{n=-\infty}^{\infty} \sum_{m=1}^{N_p} \int_{-\infty}^{\infty} Q_m(t')\,\delta\left(t - t' - \frac{nmL}{N_p v}\right) dt', \tag{4.6}$$

where $Q_m(t') = dq_m/dt'$ is the longitudinal profile of charge in the m^{th} bunch. The frequency spectrum may be obtained from the Fourier transform of the current:

$$\begin{aligned}\hat{\imath}(\omega) &= \sum_{m=1}^{N_p} \sum_{n=-\infty}^{\infty} \int_{-\infty}^{\infty}\int_{-\infty}^{\infty} e^{-j\omega t}\,Q_m(t')\,\delta\left(t - t' - \frac{nmL}{N_p v}\right) dt'\,dt, \\ &= \sum_{m=1}^{N_p} \sum_{n=-\infty}^{\infty} \hat{Q}_m(\omega) \exp\left(-j\frac{nmL}{N_p v}\omega\right). \end{aligned} \tag{4.7}$$

When the bunches are identical this becomes:

$$\hat{\imath}(\omega) = \hat{Q}(\omega) \sum_{n=-\infty}^{\infty} \exp\left(-j\frac{nL}{N_p v}\omega\right) = \frac{Q(\omega)}{N_p \omega_s} \sum_{n=-\infty}^{\infty} \delta\left(\omega - nN_p\omega_s\right) \tag{4.8}$$

with $\omega_o = 2\pi v/L$ being the angular revolution frequency.

If we approximate the bunch shape by a delta function, then the spectrum will have a "comb"-shape as shown in Fig. (4.1).

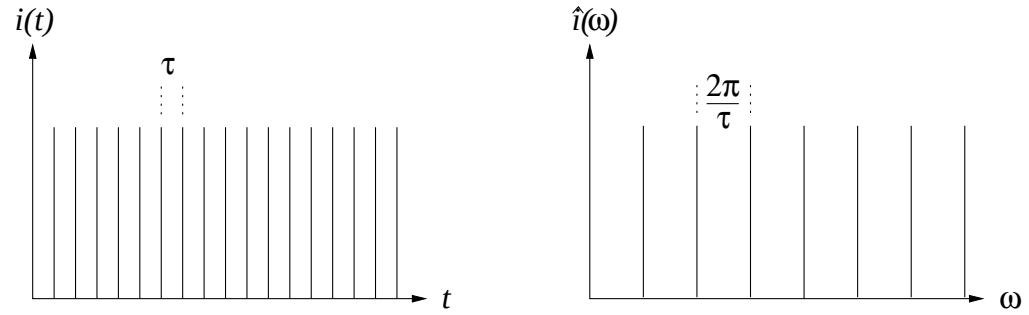

Figure. 4.1 The left plot shows the current distribution for equal δ-function bunches of charge $Q_m(t') = q\delta(t')$) and spacing $\tau = L/N_p v$. The right plot shows the corresponding Fourier transform.

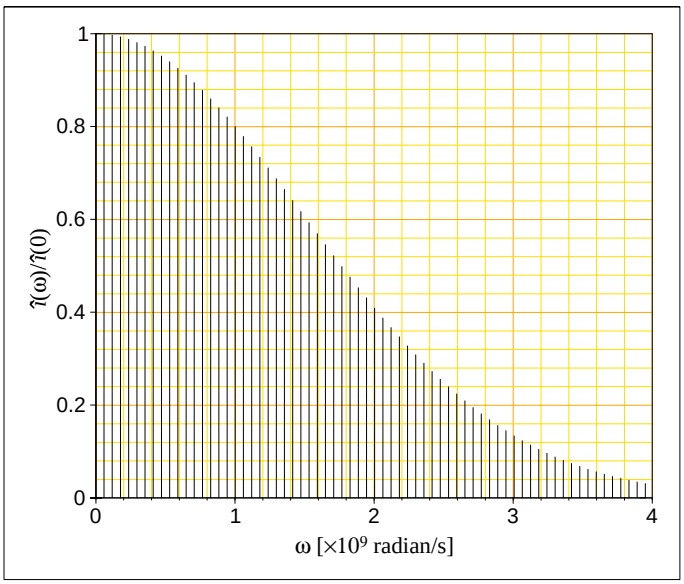

Figure. 4.2 Relative frequency of equal Gaussian bunches with 106.6 ns spacing between bunches.

If we now allow a gap in the number of bunches so that only N_b bunches are placed with the same spacing leaving $N_p - N_b$ holes in the bunch train, we should expect to see additional harmonics of the revolution lines between those of Eq. (4.8). Consider N_b bunches of equal charge q and width σ placed in N_p equally spaced buckets:

$$i(t) = \sum_{n=-\infty}^{\infty} \sum_{m=1}^{N_b} \int_{-\infty}^{\infty} \int_{-\infty}^{\infty} e^{-j\omega t} \frac{q}{\sqrt{2\pi}\sigma} e^{-\frac{t'^2}{2\sigma^2}} \, \delta\left(t - t' - \frac{nm}{N_p}\tau_s\right) dt' dt. \quad (4.8)$$

The frequency spectrum is then

$$\begin{aligned}
\hat{\imath}(\omega) &= q e^{-\frac{\sigma^2\omega^2}{2}} \sum_{n=-\infty}^{\infty} \sum_{m=1}^{N_b} \int_{-\infty}^{\infty} e^{-j\omega t} \, \delta\left(t - \frac{nm}{N_p}\tau_s\right) dt \\
&= q e^{-\frac{\sigma^2\omega^2}{2}} \sum_{n=-\infty}^{\infty} \sum_{m=1}^{N_b} e^{-j\frac{nm\omega\tau_s}{N_p}} \\
&= q e^{-\frac{\sigma^2\omega^2}{2}} \sum_{n=-\infty}^{\infty} e^{-j\frac{n\omega\tau_s}{N_p}} \frac{1 - e^{-j\frac{nN_b\omega\tau_s}{N_p}}}{1 - e^{-j\frac{n\omega\tau_s}{N_p}}} \\
&= q e^{-\frac{\sigma^2\omega^2}{2}} \sum_{n=-\infty}^{\infty} e^{-j\frac{n\omega\tau_s}{N_p}} \frac{e^{-j\frac{nm\omega\tau_s}{2N_p}}}{e^{-j\frac{n\omega\tau_s}{2N_p}}} \frac{2j\left(e^{j\frac{nN_b\omega\tau_s}{2N_p}} - e^{-j\frac{nN_b\omega\tau_s}{2N_p}}\right)}{2j\left(e^{j\frac{n\omega\tau_s}{2N_p}} - e^{-j\frac{n\omega\tau_s}{2N_p}}\right)}
\end{aligned}$$

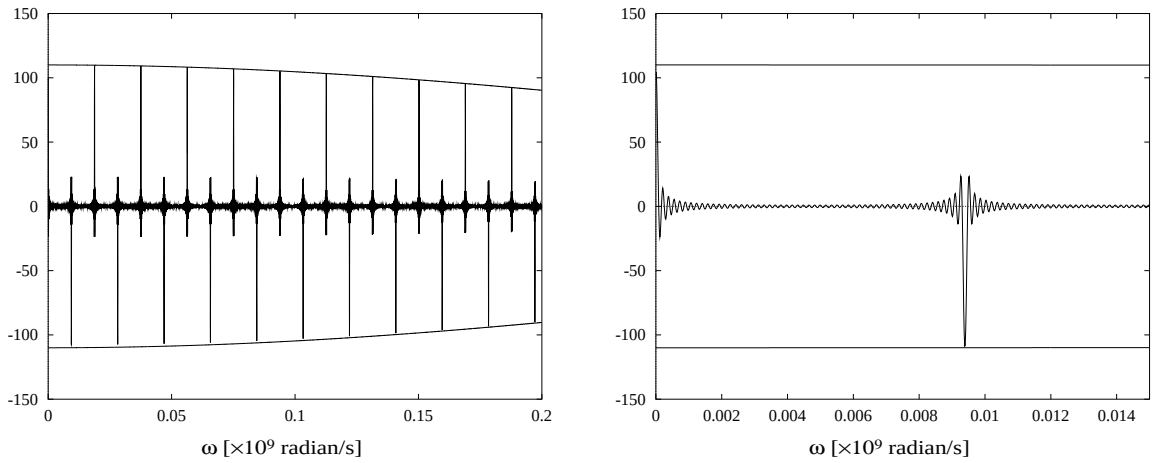

Figure. (4.3) Plot of the enhancement function times the envelope $\exp(-\sigma^2\omega^2/2)$ for $N_p = 120$, $N_b = 110$, $\tau_s = 12.7$ μs. The envelope function is plotted to guide the eye. The enlargement on the right shows the ripple caused by the gap of 10 missing bunches at a frequency of 78 kHz.

$$= qe^{-\frac{\sigma^2\omega^2}{2}} \sum_{n=-\infty}^{\infty} \frac{\sin\left(\frac{nN_b\omega\tau_s}{2N_p}\right)}{\sin\left(\frac{n\omega\tau_s}{2N_p}\right)} e^{-j\frac{n(N_b+1)\omega\tau_s}{2N_p}}$$

The modulation factor, called the *enhancement* function, is

$$\mathcal{E}_n(\omega) = \frac{\sin\left(\frac{nN_b\tau_s}{2N_p}\omega\right)}{\sin\left(\frac{n\tau_s}{2N_p}\omega\right)}. \tag{4.9}$$

From this we see that having an irregular pattern of bunches will produce more closely spaced lines separated by the revolution frequency $(1/\tau_s)$ which is smaller than the typical bunch frequency (N_p/τ_s). Other enhancement factors can be calculated for bunches of differing intensity or with more gaps between bunch trains.

4.2 Momentum spread

So far we have assumed that the particles are all oscillating at the same frequency. In fact any real beam has a nonzero momentum spread, and unless we have an isochronous ring, there will be a spread in the revolution frequencies of the individual particles. In the case of beams bunched by rf cavities, there will be synchrotron oscillations with each individual particle having a varying revolution period.

4.2.3 Longitudinal Schottky spectrum of an unbunched beam

The current of the m^{th} particle can be written as

$$\begin{aligned} i_m(t) &= q f_m \sum_{n=-\infty}^{\infty} e^{jn[\omega_m t+\psi_m]} \\ &= q f_m \left[1 + 2\sum_{n=1}^{\infty} \cos[n(\omega_m t + \psi_m)]\right] \end{aligned} \tag{4.10}$$

where $f_m = \omega_m/2\pi$ and ψ_m are the respective revolution frequency and phase of the particle.

Averaging over N particles in the beam the rms frequency spread of the n^{th} revolution harmonic of the synchronous particle's frequency f_s will be the absolute value of

$$\text{harmonic bandwidth} = n\sigma_f = n f_s \, |\eta_{\text{tr}}| \frac{\sigma_p}{p}, \tag{4.11}$$

where we recall that the phase slip factor was defined in Ref. [2] as

$$\eta_{\text{tr}} = \frac{1}{\gamma^2} - \frac{1}{{\gamma_{\text{tr}}}^2}. \tag{4.12}$$

The total average current for a large number of particles is

$$\langle i \rangle = \sum_{i=1}^{N} i_m(t) = Nq\langle f \rangle = Nq f_s, \tag{4.13}$$

which is just the dc component of the current. The rms component of current may be found from

$$\begin{aligned} \sigma_i^2 &= \left\langle (i - \langle i \rangle)^2 \right\rangle \\ &= \left\langle \left[\sum_{m=1}^{N} q f_m \left(1 + 2\sum_{n=1}^{\infty} \cos(n\omega_m t + \psi_m)\right) - Nq f_s \right]^2 \right\rangle \\ &= 2q^2 f_s^2 N. \end{aligned} \tag{4.14}$$

So the rms current component is then

$$\sigma_i = q f_s \sqrt{2N}, \tag{4.15}$$

which is independent of harmonic number. The bandwidth is however proportional to the number n of the revolution harmonic as given by Eq. (4.11) and indicated in Fig. (4.4).

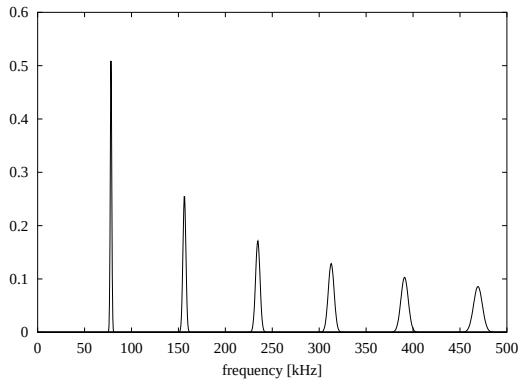

Figure. 4.4 Plot of first six revolution harmonics. (I have exaggerated the momentum spread so that the widths can be seen.) Note that the area under each peak (i.e., peak times width) is constant.

4.2.4 Synchrotron oscillations of a single particle

For simplicity, consider only a single particle which is now undergoing a small synchrotron oscillation. This modulates the arrival time at the detector as

$$t \to t + a\sin(\Omega_s t + \psi), \tag{4.16}$$

where a ($\ll \tau_s$) and ψ are respectively the amplitude and phase of modulation. The current seen by the detector on the n^{th}-turn is then

$$\begin{aligned} i_n &= \sum_{n=-\infty}^{\infty} q\,\delta\left(t - n\left[\tau_s + a\sin(\Omega_s n\tau_s + \psi)\right]\right) \\ &\simeq \frac{q}{\tau_s}\sum_{n=-\infty}^{\infty} e^{jn\omega_s[\tau_s + a\sin(n\Omega_s\tau_s+\psi)]}, \end{aligned} \tag{4.17}$$

where we have made use of the identity

$$\sum_{-\infty}^{\infty}\delta(t - n\tau) = \frac{1}{\tau}\sum_{-\infty}^{\infty} e^{j\frac{n2\pi t}{\tau}}. \tag{4.18}$$

Recalling another identity

$$e^{jz\sin\theta} = \sum_{m=-\infty}^{\infty} J_m(z)\,e^{j\theta}, \tag{4.19}$$

we may now write

$$i_n = q\sum_{n=-\infty}^{\infty} e^{-jn\omega_s\tau_s}\sum_{m=-\infty}^{\infty} J_m(n\omega_s a)\,e^{-jm(n\omega_s\tau_s+\psi)}. \tag{4.20}$$

Now each revolution harmonic gets split into a sequence of synchrotron satellites of relative height $J_m(a)$ for the m^{th} satellite. Since $J_m(n\omega_s a)$ decreases with increasing m only the nearest lines are important. As a rule of thumb, lines with $m \gtrsim n\, 2a\omega_s$ are negligible[1].

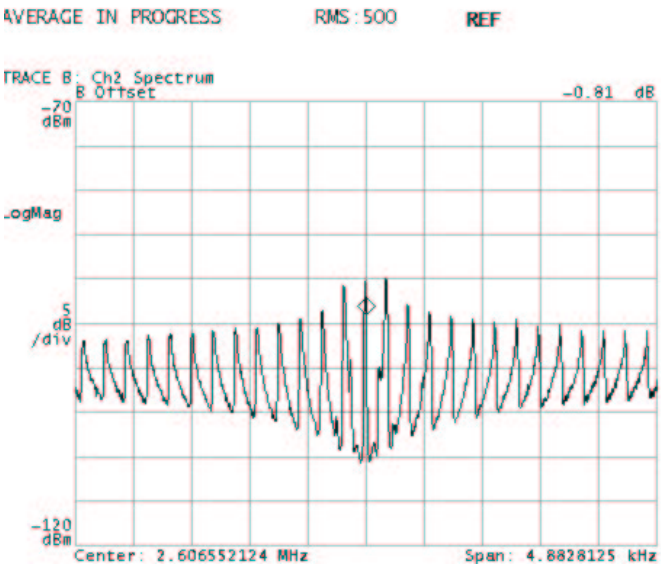

Figure. 4.5 Longitudinal spectrum showing synchrotron sidebands of a high order revolution line in RHIC. The pickup was a small Schottky cavity with a resonant frequency near 2 GHz. The signal was mixed down to the lower range of the spectrum analyzer. The peak in the middle is a revolution line of infinitesimal width, although the spike as measured does not go to infinity due to the finite bandwidth of the analyzer. The characteristic shape of the sidebands, as having a sharp edge away from the revolution line with a sloping fall towards the revolution line, is due to the fact that the synchrotron frequency is a maximum at the center of the bucket, where the particle distribution also peaks, and then falls off toward the edge of the bucket.

4.3 Transverse Schottky spectra

4.3.5 Transverse spectrum of an unbunched beam

Again we first consider a single particle with a betatron oscillation in one plane. Here we must use a transverse pickup which is sensitive to the amplitude a_m of the oscillation. The measured signal is then proportional to the dipole oscillation signal

$$d_m = a_m(t) i_m(t), \tag{4.21}$$

for the m^{th} particle. We immediately see that the signal is proportional to both the amplitude of oscillation and to the current of the bunch, so in addition to the

effect of betatron oscillations, transverse spectra may also exhibit aspects of the longitudinal spectra. For the betatron oscillation we have

$$a_m(t) = a_m \cos(\mathrm{q}_m \omega_m t + \psi_m), \tag{4.22}$$

where q_m is the fractional part of the betatron tune, and $\omega_m/2\pi$ and ψ_m are respectively the particle's revolution frequency and betatron-phase offset. Eq. (4.21) now becomes

$$\begin{aligned} d_m(t) &= a_m \cos(\mathrm{q}_m \omega_m t + \psi_m)\, q f_m \sum_{n=-\infty}^{\infty} e^{jn\omega_m t} \\ &= \frac{q a_m f_m}{2} \left(e^{j(\mathrm{q}_m \omega_m t + \psi_m)} + e^{-j(\mathrm{q}_m \omega_m t + \psi_m)} \right) \sum_{n=-\infty}^{\infty} e^{jn\omega_m t} \\ &= \frac{q a_m f_m}{2} \sum_{n=-\infty}^{\infty} \left(e^{j[(n+\mathrm{q}_m)\omega_m t + \psi_m]} + e^{j[(n-\mathrm{q}_m)\omega_m t - \psi_m]} \right) \\ &= \frac{q a_m f_m}{2} \sum_{n=-\infty}^{\infty} \left(e^{j[(n+\mathrm{q}_m)\omega_m t + \psi_m]} + e^{-j[(n+\mathrm{q}_m)\omega_m t + \psi_m]} \right) \\ &= q a_m f_m \sum_{n=-\infty}^{\infty} \cos[(n+\mathrm{q}_m)\omega_m t + \psi_m]. \end{aligned} \tag{4.23}$$

So the spectrum will have lines spaced like the revolution harmonics but offset by an amount $\mathrm{q}_m f_m$. Since we cannot tell the difference between negative and positive frequencies, the negative frequencies fold over to give lines at $(n \pm \mathrm{q}_m) f_m$ as shown in Fig. (4.6).

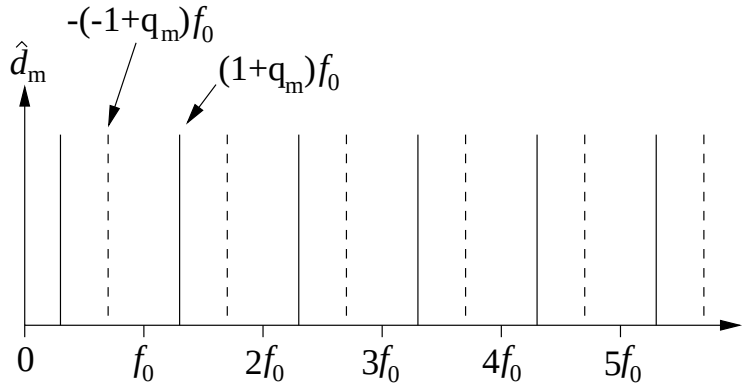

Figure. 4.7 Spectrum of betatron lines. The dashed lines are folded over from negative frequencies by plotting the absolute value $|(n+\mathrm{q})f_s|$. Here I have plotted lines for $\mathrm{q} < 0.5$.

Summing over N particles we get the total average transverse signal

$$\langle d \rangle = 0, \tag{4.24}$$

with the rms spread

$$\sigma_d = \sqrt{\langle (d_m - \langle d_m \rangle)^2 \rangle} = q f_s \, \sigma_a \sqrt{\frac{N}{2}}, \tag{4.25}$$

where σ_a is the rms betatron amplitude. The Schottky power in each sideband is proportional to σ_d^2 and is again independent of the revolution harmonic number n.

Comparing Eqs. (4.15 & 4.25) we see that the rms betatron amplitude may be obtained from

$$\sigma_a = \frac{2\sigma_d}{\sigma_i}. \tag{4.26}$$

If the detectors are very well calibrated, then this can be used to obtain the transverse emittance.

The momentum spread and betatron tune spread contribute to give a nonzero width to the betatron line. If the betatron tune spread is only due to chromaticity, then

$$\sigma_{\rm q} = |(n + {\rm q})\eta_{\rm tr} + Q\xi| \, \frac{\sigma_p}{p}, \tag{4.27}$$

where Q is the total betatron tune (including integer part) and ξ is the chromaticity

$$\xi = \frac{p}{Q} \, \frac{dQ}{dp}. \tag{4.28}$$

Other contributions to the betatron tune spread which are not chromatic should be added in quadrature with Eq. (4.27), since they would be independent of the momentum oscillation.

For large values of n, the fractional part of the tune becomes negligible and the width of the band is

$$\sigma_{\rm q} \simeq |n\eta_{\rm tr} + Q\xi| \, \frac{\sigma_p}{p}, \tag{4.29}$$

We now see that the widths of the upper and lower sidebands are different since n can be either positive or negative. Whether the upper is narrower or wider depends on the signs of $\eta_{\rm tr}$, n, and ξ.

4.3.6 Transverse spectrum of a single bunch

As alluded to in the previous section, the transverse oscillation in Eq. (4.21) is modulated by the bunch current, so we should expect to see the additional structure of the longitudinal spectra superimposed on the betatron lines of the previous section.

Due to a lack of time, I will defer the development of this section to the future. There is probably more in this chapter than we will cover in class anyway. I recommend Boussard's article[1] for more information. I have added a few pictures of Schottky measurements from RHIC showing the betatron sidebands.

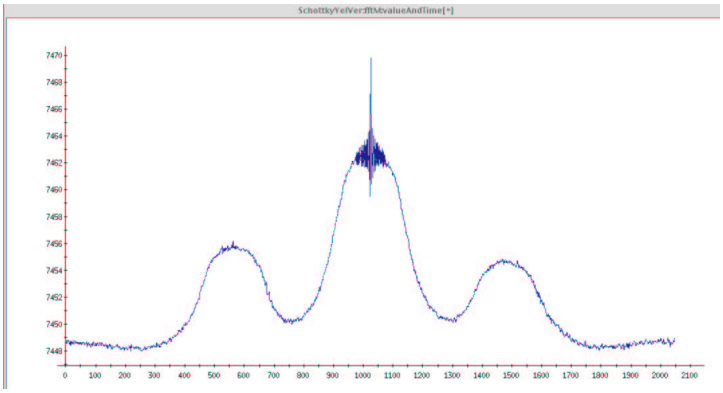

Figure. 4.8 Transverse Schottky spectrum from RHIC. The middle rounded bump is generated by the synchrotron sidebands which were not resolved by the bandwidth of the scope. The lower bumps to either side are the betatron sidebands. Unfortunately, the program used to plot this did not label the axes in physical units. The width of horizontal scale is about the revolution frequency, 78 kHz.

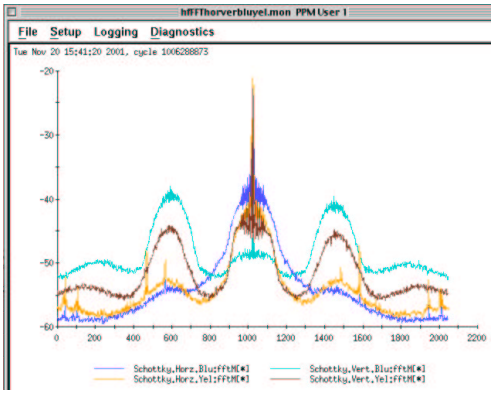

Figure. 4.9 Simultaneous Schottky signals measured for horizontal and vertical transverse motion in both the RHIC rings.

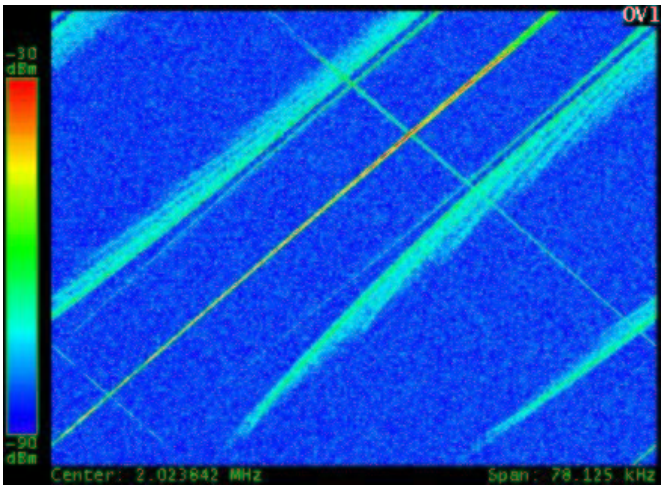

Figure. 4.10 Waterfall plot of transverse Schottky spectra of gold beam in RHIC during an energy ramp. Time increases from the top to the bottom, and individual Schottky spectra measurements are plotted horizontally. The thin straight line moving to the left (from upper right to lower left) is a revolution line. The next broad lines to either side are betatron sidebands. At the lower right there is just a hint of the next higher revolution line, with one of its corresponding betatron sideband lines. Notice how the betatron sidebands are filamenting as beam is slowly lost. The other two faint lines moving to the right are interference artifacts, probably from some signal leaking into the mixer.

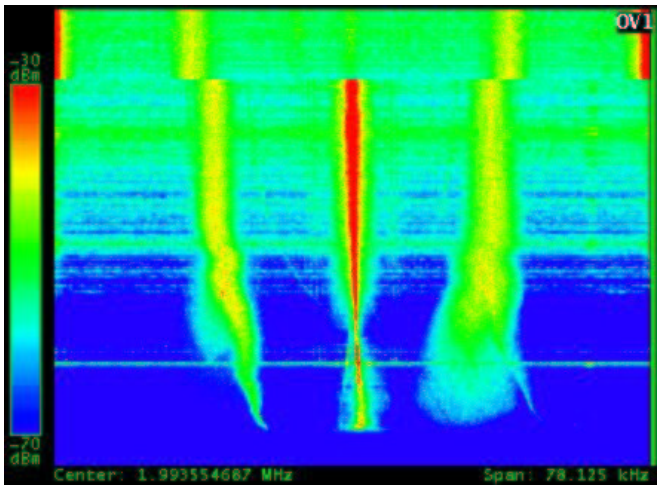

Figure. 4.11 Transverse Schottky waterfall plot during another ramp showing a revolution line in the center with two betatron sidebands. One can see that one sideband is broadening which indicates an increase in chromaticity. Again the beam was lost before the end of the ramp. (At the top you can see two revolution lines at the two edges. I'm not sure why the lines shift by half a revolution line spacing about a sixth of the way down. Presumably the reference frequency to the mixer jumped. I must investigate this. Perhaps it might be related to the phase jump at transition?) The horizontal lines (bands) in the top half show that there was a lot of broad spectrum power in the beam which is quite common, particularly before and just after transition.

References for Chapter 4

[1] D. Boussard, "Schottky Noise and Beam Transfer Function Diagnostics", *CERN Accelerator School Fifth Advanced Accelerator Physics Course*, CERN 95-06, vol. II p749 (1993).

[2] M. Conte and W. W. MacKay, *An Introduction to the Physics of Particle Accelerators*, World Scientific, Singapore (1991).

5

Leapfrog Integration of Equations of Motion

When we write simulation codes to integrate a system of equations of motion like

$$\frac{d\phi}{dt} = \alpha W \tag{5.1a}$$

$$\frac{dW}{dt} = -\beta\phi, \tag{5.1b}$$

where α and β are constants, things sometimes go awry. An obvious way to solve this without computers is to write a second order differential equation:

$$\frac{d^2\phi}{dt^2} + \alpha\beta\,\phi = 0, \tag{5.2}$$

with solutions which are sine-like or exponential depending on the sign of $\alpha\beta$. For the case of $\omega^2 = \alpha\beta > 0$ we have

$$\phi(t) = \phi_0 \cos[\omega(t - t_0)],$$

which is periodic so that a particle traces out an ellipse in the (ϕ, W)-phase space.

We frequently resort to integrating by stepping through a pair of difference equations. A simple naive approach may run into problems. First I will demonstrate the incorrect method with what might appear at first to be a reasonable choice of difference equations:

$$\phi_{n+1} = \phi_n + \alpha W_n\,\Delta t \tag{5.3a}$$

$$W_{n+1} = W_n - \beta\phi_n \Delta t, \tag{5.3b}$$

Writing them in matrix form we have

$$\begin{pmatrix} \phi_{n+1} \\ W_{n+1} \end{pmatrix} = \begin{pmatrix} 1 & \alpha\Delta t \\ -\beta\Delta t & 1 \end{pmatrix} \begin{pmatrix} \phi_n \\ W_n \end{pmatrix} = \mathbf{M} \begin{pmatrix} \phi_n \\ W_n \end{pmatrix}, \tag{5.4}$$

where the

$$\det(\mathbf{M}) = 1 + \alpha\beta\Delta t^2 \neq 1 \tag{5.5}$$

unless either α or β are zero. For $\omega^2 = \alpha\beta > 0$ this would give results with the particle proceeding to larger amplitudes in phase space instead of tracing out an ellipse. The resulting integration is nonsymplectic.

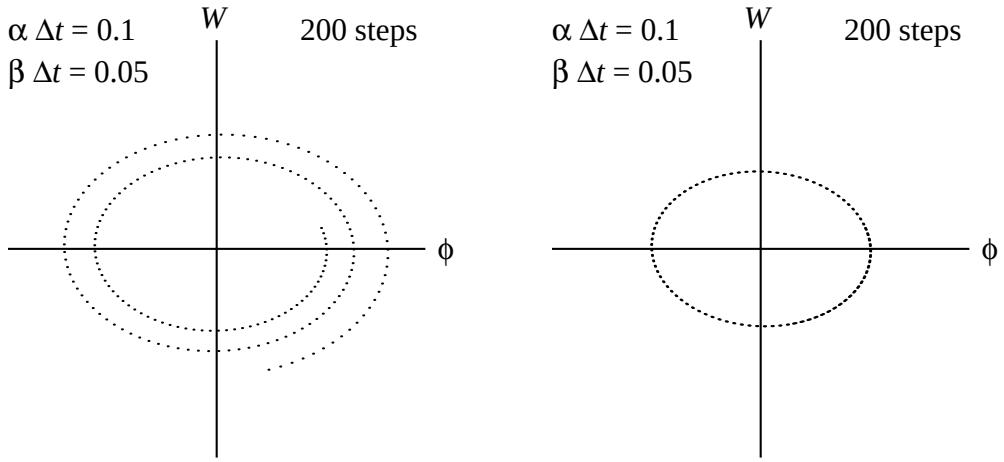

Figure. (5.1) The plot on the left shows how the improper method causes a blowup of the oscillation, whereas the plot on the write was tracked with the leap-frog method.

$$\phi_{\frac{1}{2}} \longrightarrow \phi_{1+\frac{1}{2}} \longrightarrow \phi_{2+\frac{1}{2}}$$
$$W_1 \longrightarrow W_2 \longrightarrow W_3$$

Figure. 5.2 By integrating the variables so that the time steps hop over each other, we can obtain a symplectic result.

If instead we consider Eqs. (5.1) as modeling the longitudinal motion in a circular ring with a single rf cavity, then a convenient time step would correspond to one turn with a long drift followed by a small thin-lens-type energy kick:

$$\begin{aligned}\begin{pmatrix}\phi_{n+\frac{1}{2}}\\ W_{n+1}\end{pmatrix} &= \begin{pmatrix}1 & 0\\ -\beta\Delta t & 1\end{pmatrix}\begin{pmatrix}1 & \alpha\Delta t\\ 0 & 1\end{pmatrix}\begin{pmatrix}\phi_{n-\frac{1}{2}}\\ W_n\end{pmatrix}\\ &= \begin{pmatrix}1 & \alpha\Delta t\\ -\beta\Delta t & 1-\alpha\beta\Delta t\end{pmatrix}\begin{pmatrix}\phi_{n-\frac{1}{2}}\\ W_n\end{pmatrix}\\ &= \mathbf{M}\begin{pmatrix}\phi_{n-\frac{1}{2}}\\ W_n\end{pmatrix},\end{aligned}$$

with

$$\det(M) = 1. \tag{5.7}$$

This type of two-step integration where one variable is integrated ($\phi_{n-\frac{1}{2}} \rightarrow \phi_{n+\frac{1}{2}}$) and then the other is integrated ($W_n \rightarrow W_{n+1}$) is referred to as *leap-frog* integration, since the time steps for the two variables are interleaved as indicated by Fig. (5.2).

References for Chapter 5

[1] R. W. Hockney and J. W. Eastwood, *Computer Simulation Using Particles*, Adam Hilger, Bristol (1988).

6

Example of Coupled Bunch Instability

During one ramp of polarized protons in Yellow ring of RHIC, only one of the two 28 MHz cavities for acceleration was being powered. The tuner for the other cavity was detuned to a fixed frequency away from the proper frequency. As the beam was accelerated from 24.3 GeV at injection to 100 GeV at storage the revolution frequency shifts from $f_{\mathrm{rf},i} = 28.1297$ MHz to $f_{\mathrm{rf},f} = 28.1494$ MHz. The normal harmonic number for the 28 MHz cavities is $h = 360$. At one point in the ramp, the 358^{th} harmonic of the revolution frequency crossed the resonant frequency of the unpowered cavity initiating the multibunch instability shown in Fig. (6.1).

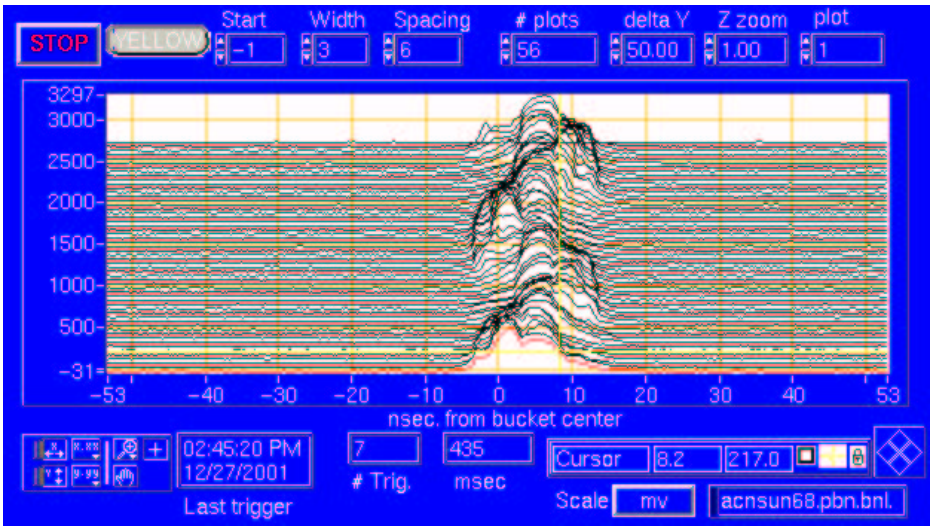

Figure. 6.1 Coupled bunch instability in the RHIC Yellow ring during acceleration of polarized protons. The 56 traces are the 55 bunches (plus one empty bucket) taken on one turn during acceleration. The populate every sixth rf bucket starting from bucket 1 up to bucket 331. There is a gap of 5 bunches (buckets 332-360) to leave room for the rise time of the abort kickers.

The bunched beam drives TM_{010} oscillations in the unpowered cavity. Each bunch will see the wake of previous bunches and gain (loose) a little energy from (to) the cavity depending on the relative phase of the wake oscillation when the bunch crosses the gap. As a result there is a slight beating of frequencies of the two cavities as indicated in Fig. (6.2).

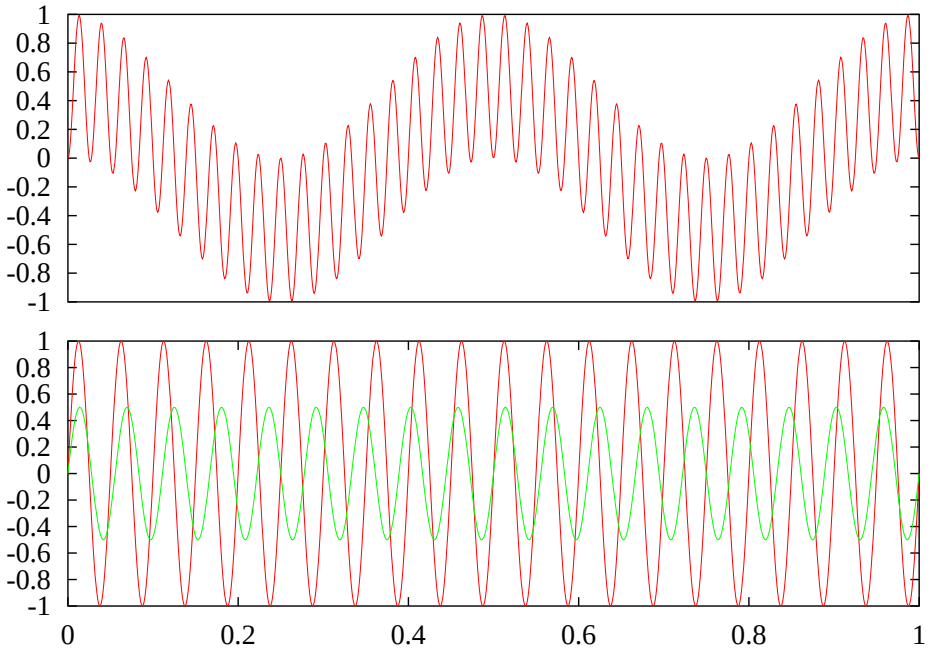

Figure. 6.2 Conceptual beating of the frequencies of the two cavities: $[\sin(2\pi hx)\sin(2\pi h'x)]$. Here the harmonic numbers $h = 20$ $[\sin(2\pi hx)]$ and $h' = 18$ $[0.5\sin(2\pi h'x)]$ were used rather than 360 and 358, so that the individual cycles could be seen for the individual cavities.

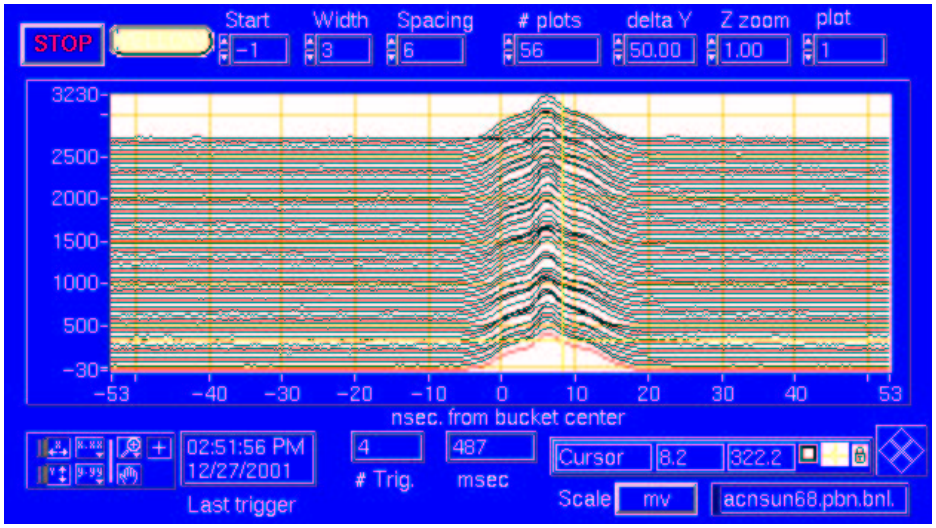

Figure. 6.3 This shows the 55 bunches later in the acceleration ramp after the oscillations have Landau damped.